Optics Letters

Wake mode sidebands and instability in mode-locked lasers with slow saturable absorbers

Shaokang Wang,[1,*] Stefan Droste,[2] Laura C. Sinclair,[2] Ian Coddington,[2] Nathan R. Newbury,[2] Thomas F. Carruthers,[1] and Curtis R. Menyuk[1]

[1]Department of Computer Science and Electrical Engineering, University of Maryland, Baltimore County, 1000 Hilltop Circle, Baltimore, Maryland 21250, USA
[2]National Institute of Standards and Technology, 325 Broadway, Boulder, Colorado 80305, USA
*Corresponding author: swan1@umbc.edu

Received 31 January 2017; revised 21 April 2017; accepted 10 May 2017; posted 11 May 2017 (Doc. ID 285829); published 14 June 2017

Passively mode-locked lasers with semiconductor saturable absorption mirrors are attractive comb sources due to their simplicity, excellent self-starting properties, and their environmental robustness. These lasers, however, can have an increased noise level and wake mode instabilities. Here, we investigate the wake mode dynamics in detail using a combination of evolutionary and dynamical methods. We describe the mode-locked pulse generation from noise when a stable pulse exists and the evolution of the wake mode instability when no stable pulse exists. We then calculate the dynamical spectrum of the mode-locked pulse, and we show that it has six discrete eigenmodes, two of which correspond to wake modes. The wake modes are unstable when the wake mode eigenvalues have a positive real part. We also show that even when the laser is stable, the wake modes lead to experimentally observed sidebands.

OCIS codes: (000.4430) Numerical approximation and analysis; (140.4050) Mode-locked lasers; (140.3425) Laser stabilization.

https://doi.org/10.1364/OL.42.002362

The search for robust, low-noise frequency comb sources has attracted significant attention during the last two decades [1–6], and numerous possibilities have been investigated. Passively mode-locked fiber lasers, in which nonlinear polarization rotation (NPR) is used as the saturable absorber mechanism [7–9], are among the most important comb sources. However, these lasers do not usually self-start, and the polarization rotation is highly sensitive to environmental disturbance [10], limiting the robustness of these lasers.

Comb lasers have been developed that are built with telecom-grade polarization-maintaining (PM) components [6,11–14], heavily doped erbium gain fiber, highly nonlinear PM fibers, and semiconductor saturable absorber mirrors (SESAMs). An example is a SESAM fiber laser that generates a highly robust 200-MHz comb [15]. It operates in the soliton regime where, to the lowest order, the pulse shape is determined by the balance between the Kerr nonlinearity and chromatic dispersion [16].

There is an important difference between NPR mode-locked lasers and SESAM mode-locked lasers. In the former case, the saturation mechanism is fast compared to the pulse duration, while in the latter case, it is slow [16,17]. The duration of pulses that are generated by SESAM fiber lasers is usually not as short as the duration of pulses from mode-locked lasers using nonlinear polarization rotation, although the output pulses can be further compressed using nonlinear amplification [3,18]. In addition, because an overall nonzero laser cavity dispersion is needed to stabilize short pulses, as discussed later, the timing jitter is usually worse than with NPR mode locking [15]. Finally, as a consequence of the slow response of the SESAM, a gain window opens up in the wake of the mode-locked pulse in which noise can grow. This noise can generate sidebands [19–21] or lead to pulse instabilities [16,19,20,22].

In this work, we use an averaged model [21] to discuss the conditions under which sidebands grow and become unstable. In contrast to prior work that either used evolutionary methods [22–25] or approximate dynamical methods based on soliton perturbation theory [16], we use computational dynamical methods [26] that allow us to unambiguously determine the source of the instability and accurately calculate the parameters of its onset. We then use evolutionary methods to determine the time evolution of the wake instability.

We briefly introduced the wake instability and the induced sidebands in prior works [19–21]. Here, we describe the pulse evolution and find the stable operating regime using an averaged model in which the effects of the laser components are averaged over one round trip. The evolution of the wave envelope is described by [16,19]

$$T_R\frac{\partial u}{\partial T}=-i\phi u+t_s\frac{\partial u}{\partial t}+\frac{g}{2}\left(1+\frac{1}{2\omega_g^2}\frac{\partial^2}{\partial t^2}\right)u-\frac{l}{2}u$$
$$-i\frac{\beta''}{2}\frac{\partial^2 u}{\partial t^2}+i\gamma|u|^2u-\frac{\rho}{2}nu, \tag{1}$$

where T_R is the round-trip time, T is the slow time of propagation, t is the retarded fast time, $u(t, T)$ is the slowly varying

field envelope, and each operator on u on the right-hand side of Eq. (1) describes its effect on the incoming pulse per round-trip: t_s is the shift in t of the pulse centroid $t_c = \int t'|u|^2 dt' / \int |u|^2 dt'$, ϕ is the phase change, g is the saturated gain, ω_g is the gain bandwidth, l is the background loss, β'' is the group-delay dispersion (GDD), γ is the Kerr nonlinearity coefficient, and ρ is the peak saturable absorption coefficient of the SESAM. We assume that the recovery time of the gain medium is significantly greater than T_R, so that the gain $g(|u|)$ is saturated by the intracavity field energy,

$$g(|u|) = g_0[1 + w_0/(P_{\text{sat}} T_R)]^{-1}, \tag{2}$$

in which g_0 is the unsaturated gain, w_0 is the intracavity pulse energy, and P_{sat} is the saturation power. We use a two-level model of the SESAM where n is the ratio of the lower level population to the total population of the SESAM. In modeling the SESAM, the parameter n obeys the equation [16]

$$\frac{\partial n(t)}{\partial t} = \frac{1 - n}{T_A} - \frac{|u(t)|^2}{w_A} n, \qquad n(-T_R/2) = 0, \tag{3}$$

where we assume that the response time $T_A \ll T_R$, and w_A is the saturation energy of the SESAM.

The quantities ϕ and t_s represent a phase shift and a time shift per round-trip. Due to the phase and time invariance of Eq. (1), these quantities have no impact on the intensity profile of the mode-locked pulse solution. When studying mode locking analytically [27] or using computational evolutionary approaches [28], it is conventional to set these quantities to zero. In that case, for most choices of the parameters, there is no solution to Eq. (1) that is strictly stationary, i.e., $\partial u/\partial T = 0$, and one searches for a solution to this equation with a steady phase rotation and/or drift. In the dynamical approach [21,26], it is convenient to choose ϕ and t_s so that the mode-locked pulse is strictly stationary, and there is no phase rotation and no shift in the central time.

The laser design follows Ref. [9] but with a repetition frequency $1/T_R = 300\,\text{MHz}$. We experimentally measure $\beta'' = -0.014\,\text{ps}^2$ and $P_{\text{sat}} = 9.01\,\text{mW}$ (see Fig. 6). We estimate $l = 1.05$ and $\gamma = 0.0011\,\text{W}^{-1}$, and we have $T_A = 2.0\,\text{ps}$ and $\rho = 0.073$ [29]. The SESAM saturation energy is $\omega_A = \Phi_{\text{sat}} A_{\text{eff,SESAM}} = 157\,\text{pJ}$, based on the reported saturation fluence $\Phi_{\text{sat}} = 50\,\text{mJ/cm}^2$ [29] and measured spot area $A_{\text{eff,SESAM}} = 314\,\text{mm}^2$. Finally, we set $g_0 = 7.74$ and $\omega_g = 30\,\text{ps}^{-1}$ to match the measured output power.

We use a modified split-step Fourier method [28] to solve Eq. (1) evolutionarily. Starting from noise, we obtain the evolution profile that is shown in Fig. 1. Due to the asymmetric temporal response of the SESAM, the cavity net gain $G_n = \exp[g(|u|) - l - \rho n(t)]$ is also asymmetric as shown in Fig. 2, and thus the centroid t_c in the computational time window moves. We have removed the centroid motion in Fig. 1. In Fig. 1(a) we show that a stable mode-locked pulse appears after about 500 round-trips (1.67 μs). In the frequency domain, shown in Fig. 1(b), only a narrow spectrum is present under the gain peak—corresponding to a noisy continuous wave—for about 250 round-trips. At that point, the power in the exponentially growing noise is sufficiently large that sidebands are generated nonlinearly, and a stable pulse forms.

The full width half-maximum (FWHM) of the stable pulse in Fig. 2 is 254 fs, the peak amplitude is 25.0 $\text{W}^{1/2}$, and the pulse energy is 181 pJ. The experimentally measured average laser output power is 4.88 mW with a pump power of 234 mW. The output coupling ratio is 9% [15], from which we estimate that the cavity pulse energy is 185 pJ. The difference in the pulse energy between our simulation and the experiment is less than 3%.

Due to the slow response of the SESAM relative to the pulse duration, a net gain window exists in the wake of the pulse that is about 2 ps in duration, as shown in Fig. 2. Wake modes can grow inside this net gain window. As they grow, we observe that dispersion carries them away from the pulse, where they ultimately experience loss. Thus, dispersion is necessary to attenuate the wake modes [19]. The long response time of the SESAM relative to the pulse duration plays an important role here. When the SESAM response time becomes comparable to the pulse duration, as is the case in picosecond bulk lasers, the wake instability is no longer observed [30].

The pulse is destabilized by the wake modes when the unsaturated gain becomes sufficiently large or the GDD becomes sufficiently small. In Fig. 3, we show an example in which g_0 is increased to 13.5. We observe a quasi-periodic evolution in the time domain as shown in Fig. 3(a). We show in four subfigures, Figs. 3(c)–3(f), an example of the amplitude evolution profile in detail. A second pulse, ②, forms in the wake of the original pulse, ①, and grows at its expense, ultimately leading to the disappearance of the original pulse. A third pulse, ③, then begins to grow in the wake of pulse ②, and the process continues indefinitely [19]. We show the frequency domain in Fig. 3(b). The spectrum has approximately the same width as in Fig. 1(b), but undergoes a complex and incoherent evolution. We show an animation of the evolution in Visualization 1. Thus, this instability sets a lower limit on the magnitude of the group velocity dispersion and an upper limit on the pump power (unsaturated gain) for stable operation, which therefore sets a lower limit on the pulse duration and an upper limit on the pulse energy. Hence, mode-locked lasers that use

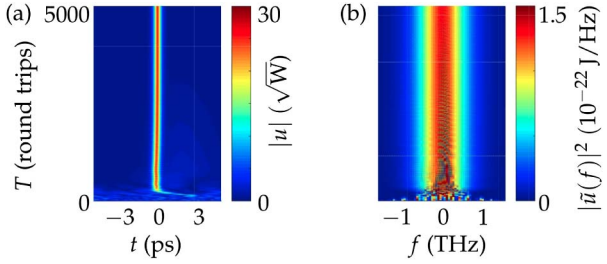

Fig. 1. Starting from noise, the system of Eq. (1) evolves to a stable profile in the (a) time domain, (b) frequency domain, where $\tilde{u}(f) = \int_0^{T_R} u(t) \exp(-i\omega t) dt$.

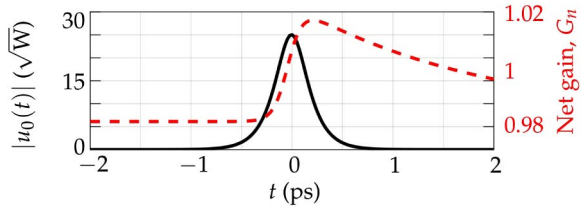

Fig. 2. Stationary pulse u_0 and the net gain, $G_n = \exp[g(|u_0|) - l - \rho n(t)]$, which exhibits an asymmetric profile due to the SESAM. A net gain window exists when $G_n > 1$.

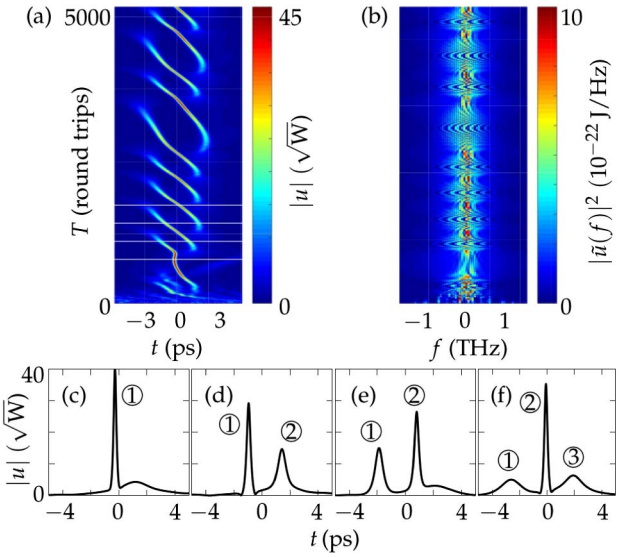

Fig. 3. Evolution profile of the wake mode instability (a) in the time domain, and (b) in the frequency domain (see Visualization 1), and the pulse amplitude profile at (c) $T = 823$, (d) $T = 948$, (e) $T = 1073$, and (f) $T = 1198$. The locations of profiles (c), (d), (e), and (f) are marked by white lines in (a).

slow saturable absorbers generally become unstable as the group delay dispersion approaches zero. By contrast, lasers using fast saturable absorbers can operate with net zero dispersion [31–34].

We can accurately determine the threshold for the onset of the wake instability by using computational dynamical methods, i.e., the boundary tracking algorithms that are described in [21,26]. In this approach, we find a stationary solution $[u_0, \phi, t_s]$ of Eq. (1), which corresponds to a mode-locked pulse. We then linearize Eq. (1) about this solution, and we determine the eigenvalues (dynamical spectrum) and eigenvectors of this linearized equation. Determining this dynamical spectrum is mathematically analogous to finding the eigenvalues and eigenmodes of an active waveguide.

In Fig. 4, we show the dynamical spectrum near the origin of the complex plane for the SESAM laser. Resembling the

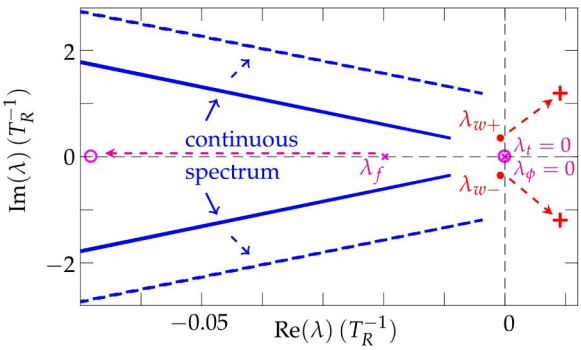

Fig. 4. Variation of the dynamical spectrum when the unsaturated gain g_0 increases from 1.90 to 2.70. We find that $\lambda_{w\pm} = -7.75 \times 10^{-4} \pm 0.352i$ when $g_0 = 7.74$ and $\lambda_{w\pm} = 9.09 \times 10^{-3} \pm 1.19i$ when $g_0 = 13.5$. The dashed arrows indicate how the spectrum shifts as g_0 increases from 7.74 to 13.5. The eigenvalue $\lambda_a < -0.90$ is not shown here.

dynamical spectrum of classical soliton perturbation theory [35], the spectrum has two branches corresponding to continuous wave perturbations, as well as four discrete eigenvalues that correspond to perturbations of the stationary pulse's central time (λ_t), central phase (λ_ϕ), central frequency (λ_f), and amplitude (λ_a), respectively. However, there are two additional discrete eigenvalues λ_{w+} and λ_{w-} that correspond to the wake modes [21], as shown in Fig. 4.

If any eigenvalues in the dynamical spectrum have a positive real part, then the stationary pulse is unstable [26]. Both λ_t and λ_ϕ remain at the origin due to the time and phase invariance of Eq. (1). We see from Fig. 4 that when $g_0 = 7.74$, the real parts of the continuous spectrum are negative and the discrete eigenvalues λ_f and λ_a are both negative. In addition, the wake mode eigenvalues $\lambda_{w\pm} = -7.75 \times 10^{-4} \pm 0.352i$, as shown in Fig. 4. Hence, the system is stable and close to the stability boundary in the parameter space. The wake modes are bounded modes with a very slow decay rate in T [21].

The stationary pulse becomes unstable when the unsaturated gain g_0 becomes sufficiently large. In Fig. 4, we use dashed arrows to show how the dynamical spectrum shifts when g_0 increases up to 13.5. We find that all eigenvalues have negative real parts except the wake mode eigenvalues, for which $\lambda_{w\pm} = 9.09 \times 10^{-3} \pm 1.19i$. The positive real part of $\lambda_{w\pm}$ indicates that the wake modes will grow, destabilizing the stationary pulse.

In Fig. 5, we show the stable regions in the (g_0, β'') parameter space. When the group delay dispersion coefficient β'' varies from -0.03 ps^2 to zero, there exist two stability boundaries. For a given value of β'', when g_0 becomes sufficiently small, the pulse becomes unstable due to the background radiation (continuous modes) [26], i.e., the system gain is below the mode-locking threshold. When g_0 becomes sufficiently large, the pulse becomes unstable due to the wake modes. The instability threshold for g_0 decreases as the system approaches zero dispersion. When $\beta'' = 0$, the pulse is, in principle, stable in a very narrow range of g_0, $1.14 < g_0 < 1.18$. In practice, this range is so narrow that a laser operating within it would be destabilized by noise and other perturbations. In addition, the pulse width of the stationary pulse is $\tau_0 > 3$ ps, which is longer than the SESAM recovery time, $T_A = 2$ ps. This operating state of the SESAM is inefficient because the saturable absorption experienced by the pulse is strongly offset by the lower-level population recovery.

The real parts of the dynamical spectrum that we show in Fig. 4 indicate the growth rate of the eigenmodes, while the imaginary part of the spectrum indicates their phase shift

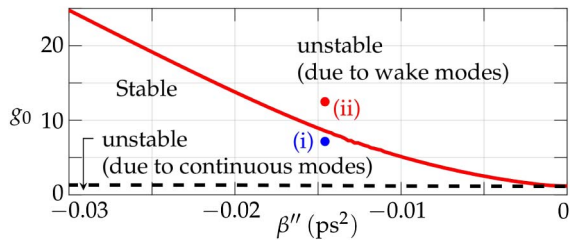

Fig. 5. Stability boundaries in the parameter space of the unsaturated gain g_0 and the group velocity dispersion β''. The points (i) and (ii) indicate the cases $g_0 = 7.74$ and $g_0 = 13.5$, respectively, with $\beta'' = -0.0144$ ps^2.

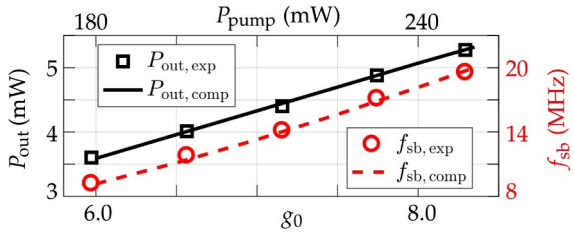

Fig. 6. Variation of the output power P_{out} and the sidebands' frequency offset f_{sb} as the unsaturated gain g_0 increases. The stationary pulse becomes unstable when $g_0 = 8.5$.

per round-trip with respect to the stationary pulse. In the presence of noise, the eigenmodes with nonzero imaginary eigenvalues introduce a frequency modulation of the mode-locked spectrum, which can be observed in the power spectrum as sidebands. We have shown the profile of the sidebands in [20] when observed using a radio frequency (RF) spectrum analyzer. These sidebands can also be observed when heterodyning the comb light with a CW laser. The frequency offset of the wake mode sidebands that is predicted from the value of the imaginary part of $\lambda_{w\pm}$ is

$$f_{\text{sb}} = \text{Im}(|\lambda_{w\pm}|)/(2\pi T_R). \quad (4)$$

In Fig. 6, we show the variation of the output power of the SESAM laser, as well as the frequency offset of the sidebands with respect to each comb line as the unsaturated gain increases. We see that, as the pump power P_{pump} increases from 180 to 250 mW, the laser output power $P_{\text{out,exp}}$ increases almost linearly from 3.6 to 5.3 mW. Meanwhile, the frequency offset of the wake mode sidebands $f_{\text{sb,exp}}$ increases from about 9 to about 20 MHz. There is good agreement between theory and experiment. We find that the laser becomes unstable due to the wake mode instability when $g_0 > 8.5$. In addition, we observe that the pump power is linearly proportional to g_0, i.e., $P_{\text{pump}} \approx 30\ \text{mW} \times g_0$. The linear scale suggests that, in this case, the upper-state population of the erbium-doped fiber is not completely depleted.

In summary, we have described the wake modes and their effect on stationary pulses in mode-locked lasers with slow saturable absorbers. A gain window forms behind the pulse, and wake modes can grow in this gain window. The mode-locked pulses become unstable when the wake modes are not swept away from the pulse by dispersion or attenuated by the background loss. Using a dynamical analysis, we show that this instability occurs when the eigenvalues in the dynamical spectrum that correspond to the wake modes have a positive real part. When the laser parameters are close to the stability boundary, the wake modes can cause sidebands in the output spectrum. We demonstrate that the dynamical spectrum can accurately predict the frequency offset of the wake mode sidebands.

Funding. Defense Advanced Research Projects Agency (DARPA) via Aviation and Missile Research, Development, and Engineering Center (AMRDEC) (W31P4Q-14-1-0002).

REFERENCES

1. S. A. Diddams, J. Opt. Soc. Am. B **27**, B51 (2010).
2. N. R. Newbury, Nat. Photonics **5**, 186 (2011).
3. S. Droste, G. Ycas, B. R. Washburn, I. Coddington, and N. R. Newbury, Nanophotonics **5**, 19 (2016).
4. N. R. Newbury and W. C. Swann, J. Opt. Soc. Am. B **24**, 1756 (2007).
5. J. Ye and S. Cundiff, *Femtosecond Optical Frequency Comb: Principle, Operation and Applications* (Springer, 2006).
6. T. R. Schibli, K. Minoshima, F.-L. Hong, H. Inaba, A. Onae, H. Matsumoto, I. Hartl, and M. E. Fermann, Opt. Lett. **29**, 2467 (2004).
7. L. Nelson, D. Jones, K. Tamura, H. Haus, and E. Ippen, Appl. Phys. B **65**, 277 (1997).
8. C.-J. Chen, P. K. A. Wai, and C. R. Menyuk, Opt. Lett. **19**, 198 (1994).
9. B. R. Washburn, R. W. Fox, N. R. Newbury, J. W. Nicholson, K. Feder, P. S. Westbrook, and C. G. Jørgensen, Opt. Express **12**, 4999 (2004).
10. B. S. Marks, T. F. Carruthers, and C. R. Menyuk, in *Conference on Lasers and Electro-Optics* (Optical Society of America, 2012), paper CTu1I.3.
11. I. Hartl, G. Imeshev, M. E. Fermann, C. Langrock, and M. M. Fejer, Opt. Express **13**, 6490 (2005).
12. H. Byun, M. Y. Sander, A. Motamedi, H. Shen, G. S. Petrich, L. A. Kolodziejski, E. P. Ippen, and F. X. Kärtner, Appl. Opt. **49**, 5577 (2010).
13. M. C. Stumpf, S. Pekarek, A. E. H. Oehler, T. Südmeyer, J. M. Dudley, and U. Keller, Appl. Phys. B **99**, 401 (2010).
14. C. Kim, K. Jung, K. Kieu, and J. Kim, Opt. Express **20**, 29524 (2012).
15. L. C. Sinclair, I. Coddington, W. C. Swann, G. B. Rieker, A. Hati, K. Iwakuni, and N. R. Newbury, Opt. Express **22**, 6996 (2014).
16. F. Kärtner, I. Jung, and U. Keller, IEEE J. Sel. Top. Quantum Electron. **2**, 540 (1996).
17. M. E. Fermann and I. Hartl, IEEE J. Sel. Top. Quantum Electron. **15**, 191 (2009).
18. C. V. Shank, R. L. Fork, R. Yen, R. H. Stolen, and W. J. Tomlinson, Appl. Phys. Lett. **40**, 761 (1982).
19. S. Wang, C. R. Menyuk, L. Sinclair, I. Coddington, and N. R. Newbury, in *Conference on Lasers and Electro-Optics* (Optical Society of America, 2014), paper SW3E.4.
20. S. Wang, C. R. Menyuk, S. Droste, L. Sinclair, I. Coddington, and N. R. Newbury, in *Conference on Lasers and Electro-Optics* (Optical Society of America, 2016), paper SM3H.5.
21. C. R. Menyuk and S. Wang, Nanophotonics **5**, 332 (2016).
22. O. G. Okhotnikov and R. Herda, Quantum Electron. **41**, 610 (2011).
23. J. N. Kutz, B. C. Collings, K. Bergman, S. Tsuda, S. T. Cundiff, W. H. Knox, P. Holmes, and M. Weinstein, J. Opt. Soc. Am. B **14**, 2681 (1997).
24. B. C. Collings, K. Bergman, S. T. Cundiff, S. Tsuda, J. N. Kutz, J. E. Cunningham, W. Y. Jan, M. Koch, and W. H. Knox, IEEE J. Sel. Top. Quantum Electron. **3**, 1065 (1997).
25. O. Shtyrina, M. Fedoruk, S. Turitsyn, R. Herda, and O. Okhotnikov, J. Opt. Soc. Am. B **26**, 346 (2009).
26. S. Wang, A. Docherty, B. S. Marks, and C. R. Menyuk, J. Opt. Soc. Am. B **31**, 2914 (2014).
27. H. A. Haus and A. Mecozzi, IEEE J. Quantum Electron. **29**, 983 (1993).
28. S. Wang, A. Docherty, B. S. Marks, and C. R. Menyuk, J. Opt. Soc. Am. B **30**, 3064 (2013).
29. SAM™ data sheet SAM-1550-21-2ps-x, λ = 1550 nm, http://www.batop.com/products/saturable-absorber/saturable-absorber-mirror/saturable-absorber-mirror-1550nm.html. Accessed on January 14, 2017.
30. U. Keller, K. J. Weingarten, F. X. Kartner, D. Kopf, B. Braun, I. D. Jung, R. Fluck, C. Honninger, N. Matuschek, and J. A. der Au, IEEE J. Sel. Top. Quantum Electron. **2**, 435 (1996).
31. Y. Shen, J. Zweck, S. Wang, and C. R. Menyuk, Stud. Appl. Math. **137**, 238 (2016).
32. N. N. Akhmediev, J. M. Soto-Crespo, and P. Grelu, Phys. Lett. A **372**, 3124 (2008).
33. Y. Song, C. Kim, K. Jung, H. Kim, and J. Kim, Opt. Express **19**, 14518 (2011).
34. L. Nugent-Glandorf, T. A. Johnson, Y. Kobayashi, and S. A. Diddams, Opt. Lett. **36**, 1578 (2011).
35. D. J. Kaup, Phys. Rev. A **42**, 5689 (1990).